

Supporting Information

Salanenka et al. 10.1073/pnas.1721760115

SI Materials and Methods

Lines. *PIN2::PIN2-GFP* (1), *pat4-1*, *pat4-1*×*PIN2-GFP* (2), *snx1-1*, *SNX-GFP* (3), *snx1-1*×*PIN2-GFP* (4), *pat3-3*, *pat3-3*×*PIN2-GFP* (5), *FYVE-GFP* (6), *ARA7-GFP* (7), *BRI1::BRI1-GFP* (8), *PGP19::PGP19-GFP* (9), *UBQ::PIPI;4-mCherry* (10), *clasp1* (11), *MAP4-GFP* (12), *EB1b-GFP* (13), *GFP-CLASPI*, *clasp1*×*PIN2-GFP* (14), quintuple *della* mutant, *pGAI::gai-1-GR* (15), *gaiΔ17* (16), *pdf3* and *pdf5* (17), *pdf6* (18), and *eir1-1* (19) were described previously. The *kin1* (SAIL_343_D12) mutant was purchased from the *Arabidopsis* Biological Resource Center, and *tor1-1* (N378) was purchased from the Nottingham *Arabidopsis* Stock Centre.

Growth Conditions. Three percent chlorine gas was used to sterilize seeds overnight. Plants were grown vertically on half-strength MS medium, including vitamins (Duchefa), with 1% (wt/vol) sucrose and 0.5 g/L 2-(*N*-morpholino) ethanesulfonic acid (pH 5.7), under a 16-h light/8-h dark photoperiod at 22/18 °C. All experiments were carried out in the light period.

Plasmid Constructs and Plant Transformation. *UBQ::VENUS:TUA6* was created using the Gateway cloning system by introducing the coding sequence of the *TUA6* gene (At4g14960) with stop codon into the pDONR P2r-P3 vector (Invitrogen). The *UBQ10* promoter was created by cloning 2 kb upstream of the start codon of the *UBIQUITIN 10* gene (AT4G05320) into the pDONRP4-P1r vector (Invitrogen). The *VENUS* sequence was cloned into pDONR221 (Invitrogen). These three fragments were then assembled into the pK7m34GW destination vector (<https://gateway.psb.ugent.be/>). Col-0 plants were transformed using standard floral dip procedures and transgenic plants were selected on MS medium +1% sucrose plates containing 50 µg/mL kanamycin. In the T2 generation, fluorescent lines that segregated as single locus were selected and propagated into the T3 generation. *pPIN2::PIN2:DENDRA* was generated by replacing the *GFP* fragment of the *pPIN2::PIN2:GFP* construct (20) with *DENDRA*. Mutant *eir1-1* plants were used for transformation and selected on BASTA. To generate *pPIN2::NLS-GFP*, 1,397 bp *PIN2* promoter sequence was cloned into pDONRP4-P1r and *NLS-GFP* coding sequence into pENTR-L1-L2. Both entry clones were assembled in pB7m24GW,3 (<https://gateway.psb.ugent.be/>) to generate the *pPIN2::NLS-GFP* expression clone, which was transformed into Col-0 plants by floral dip; positive T1 transformants and single-insert T2 lines were selected on BASTA. *pPIN2::PIN2:mCherry* was generated by replacing of the *Venus* tag with *mCherry* by cloning it via NaeI/AvrII into *pPZP-PIN2::PIN2:Venus* (20). Confirmed clones were transformed into *eir1-4* plants, and resulting T2/T3 progeny was tested for complementation and reporter expression. To generate estradiol-inducible *XVE>>PIN2-GFP*, *PIN2-GFP* fragment was cloned into pDONR221 (Invitrogen) and via LR reaction introduced into Gateway vector pMDC7 (21).

Immunolocalization of the PIN2 Protein. Antibodies were diluted as follows: 1:1,000 for anti-PIN2 serum and incubated for 4 h (1) and 1:600 for CY3-conjugated goat/anti-rabbit secondary antibody

(Dianova) and incubated for 4 h. The PM signal was measured and quantified in 16 cells per root in eight individual seedlings.

Drug Application and Experimental Conditions. Paclobutrazol [1 µM final concentration (f.c.)], GA₃ (50 µM f.c.), oryzalin (20 µM and 10 µM f.c.), BFA (50 µM f.c.), and DEX (10 µM f.c.) were used for treatments. Mock treatments were done with equal amounts of solvent (DMSO/ethanol). Double drug treatments with taxol, oryzalin, or BFA were carried out with a 30-min pretreatment followed by a concomitant drug treatment for the indicated duration. All independent experiments were done at least in triplicate, with a minimum of eight individual plants.

Dark treatments to visualize the vacuolar degradation of PIN2 were done as described previously (4). To evaluate the PIN2 amount in lytic vacuoles, a square of the size of a cell, excluding the PM, was used for quantification. Images were collected at the transition zone.

Fluorescent measurements were done on the original CLSM image files. A rectangular ROI at the PM was used for PM signal intensity quantification, and the PM signal was measured in 16 epidermal cells, including trichoblasts and atrichoblasts in eight individual roots. The intensity of the fluorescent signals was measured with the Fiji software, and the images were processed in Adobe Photoshop CS5.1 (Adobe systems). Graphs were generated with BoxPlotR (shiny.chemgrid.org/boxplotr/) or Microsoft Excel. Data represent means of eight or more roots per treatment and 16 cells per root; Student's test was used to evaluate significant differences, **P* ≤ 0.05, ***P* ≤ 0.005.

Western Blotting. The PIN2 and SNX1 protein abundance in membrane and soluble fractions were evaluated as previously described in ref. 22. For Western blot analysis of PIN2 in Col-0 plants, affinity purified rabbit anti-PIN2 serum in dilution 1:2,000 was used. A mouse monoclonal GFP antibody in dilution 1:2,000 (JL-8; Clontech) was used for GFP-tagged PIN2 and SNX1 proteins. Detection was performed using anti-rabbit or anti-mouse horseradish peroxidase-conjugated secondary antibodies (1:10,000) and enhanced chemiluminescence substrate (SuperSignal West Femto, Maximum sensitivity substrate; Thermo Scientific). Mouse anti-actin antibody (Sigma) in 1:5,000 dilution was used as an internal control. Blots were recorded on a Peqlab Fusion SL Advance Imager. The intensity of the chemiluminescent signals was measured with the Fiji software.

Quantitative RT-PCR. RNA was extracted with the RNeasy mini kit (Qiagen) from excised root tips of 5-d-old seedlings. A DNase treatment with the RNase-free DNase (Qiagen) was carried out for 15 min at 25 °C. Poly(dT) cDNA was prepared from 1 µg of total RNA with the iScript cDNA Synthesis Kit (Biorad) and analyzed on a LightCycler 480 II (SW1.5.1 Version; Roche Diagnostics) with the SYBR Green I Master kit (Roche Diagnostics) according to the manufacturer's instructions. Targets were quantified with specific primer pairs designed with the Beacon Designer 4.0 (Premier Biosoft International). All PCRs were performed in technical triplicates. Expression levels were first normalized to *UBQ10* or *PP2A* expression levels and then to the respective expression levels in mock. The primers used to quantify gene expression levels are listed in Fig. S5E.

1. Abas L, et al. (2006) Intracellular trafficking and proteolysis of the *Arabidopsis* auxin-efflux facilitator PIN2 are involved in root gravitropism. *Nat Cell Biol* 8:249–256, and correction (2006) 8:424.
2. Zwiwka M, et al. (2011) The AP-3 adaptor complex is required for vacuolar function in *Arabidopsis*. *Cell Res* 21:1711–1722.
3. Jaillais Y, Fobis-Loisy I, Miège C, Rollin C, Gaude T (2006) AtSNX1 defines an endosome for auxin-carrier trafficking in *Arabidopsis*. *Nature* 443:106–109.
4. Kleine-Vehn J, et al. (2008) Differential degradation of PIN2 auxin efflux carrier by retromer-dependent vacuolar targeting. *Proc Natl Acad Sci USA* 105:17812–17817.

5. Nodzyński T, et al. (2013) Retromer subunits VPS35A and VPS29 mediate prevacuolar compartment (PVC) function in *Arabidopsis*. *Mol Plant* 6:1849–1862.
6. Vermeer JEM, et al. (2006) Visualization of PtdIns3P dynamics in living plant cells. *Plant J* 47:687–700.
7. Ueda T, Yamaguchi M, Uchimiya H, Nakano A (2001) Ara6, a plant-unique novel type Rab GTPase, functions in the endocytic pathway of *Arabidopsis thaliana*. *EMBO J* 20:4730–4741.
8. Geldner N, Hyman DL, Wang X, Schumacher K, Chory J (2007) Endosomal signaling of plant steroid receptor kinase BRI1. *Genes Dev* 21:1598–1602.

9. Mravec J, et al. (2008) Interaction of PIN and PGP transport mechanisms in auxin distribution-dependent development. *Development* 135:3345–3354.
10. Boursiac Y, et al. (2005) Early effects of salinity on water transport in *Arabidopsis* roots. Molecular and cellular features of aquaporin expression. *Plant Physiol* 139:790–805.
11. Ambrose JC, Shoji T, Kotzer AM, Pighin JA, Wasteneys GO (2007) The *Arabidopsis* CLASP gene encodes a microtubule-associated protein involved in cell expansion and division. *Plant Cell* 19:2763–2775.
12. Marc J, et al. (1998) A *GFP-MAP4* reporter gene for visualizing cortical microtubule rearrangements in living epidermal cells. *Plant Cell* 10:1927–1940.
13. Chan J, Calder GM, Doonan JH, Lloyd CW (2003) EB1 reveals mobile microtubule nucleation sites in *Arabidopsis*. *Nat Cell Biol* 5:967–971.
14. Ambrose C, Allard JF, Cytrynbaum EN, Wasteneys GO (2011) A CLASP-modulated cell edge barrier mechanism drives cell-wide cortical microtubule organization in *Arabidopsis*. *Nat Commun* 2:430.
15. Locascio A, Blázquez MA, Alabadi D (2013) Dynamic regulation of cortical microtubule organization through prefoldin-DELLA interaction. *Curr Biol* 23:804–809.
16. Peng J, et al. (1997) The *Arabidopsis* *GAI* gene defines a signaling pathway that negatively regulates gibberellin responses. *Genes Dev* 11:3194–3205.
17. Rodríguez-Milla MA, Salinas J (2009) Prefoldins 3 and 5 play an essential role in *Arabidopsis* tolerance to salt stress. *Mol Plant* 2:526–534.
18. Gu Y, et al. (2008) Prefoldin 6 is required for normal microtubule dynamics and organization in *Arabidopsis*. *Proc Natl Acad Sci USA* 105:18064–18069.
19. Xu J, Scheres B (2005) Dissection of *Arabidopsis* ADP-RIBOSYLATION FACTOR 1 function in epidermal cell polarity. *Plant Cell* 17:525–536.
20. Leitner J, et al. (2012) Lysine63-linked ubiquitylation of PIN2 auxin carrier protein governs hormonally controlled adaptation of *Arabidopsis* root growth. *Proc Natl Acad Sci USA* 109:8322–8327.
21. Curtis MD, Grossniklaus U (2003) A gateway cloning vector set for high-throughput functional analysis of genes in plants. *Plant Physiol* 133:462–469.
22. Abas L, Luschnig C (2010) Maximum yields of microsomal-type membranes from small amounts of plant material without requiring ultracentrifugation. *Anal Biochem* 401: 217–227.

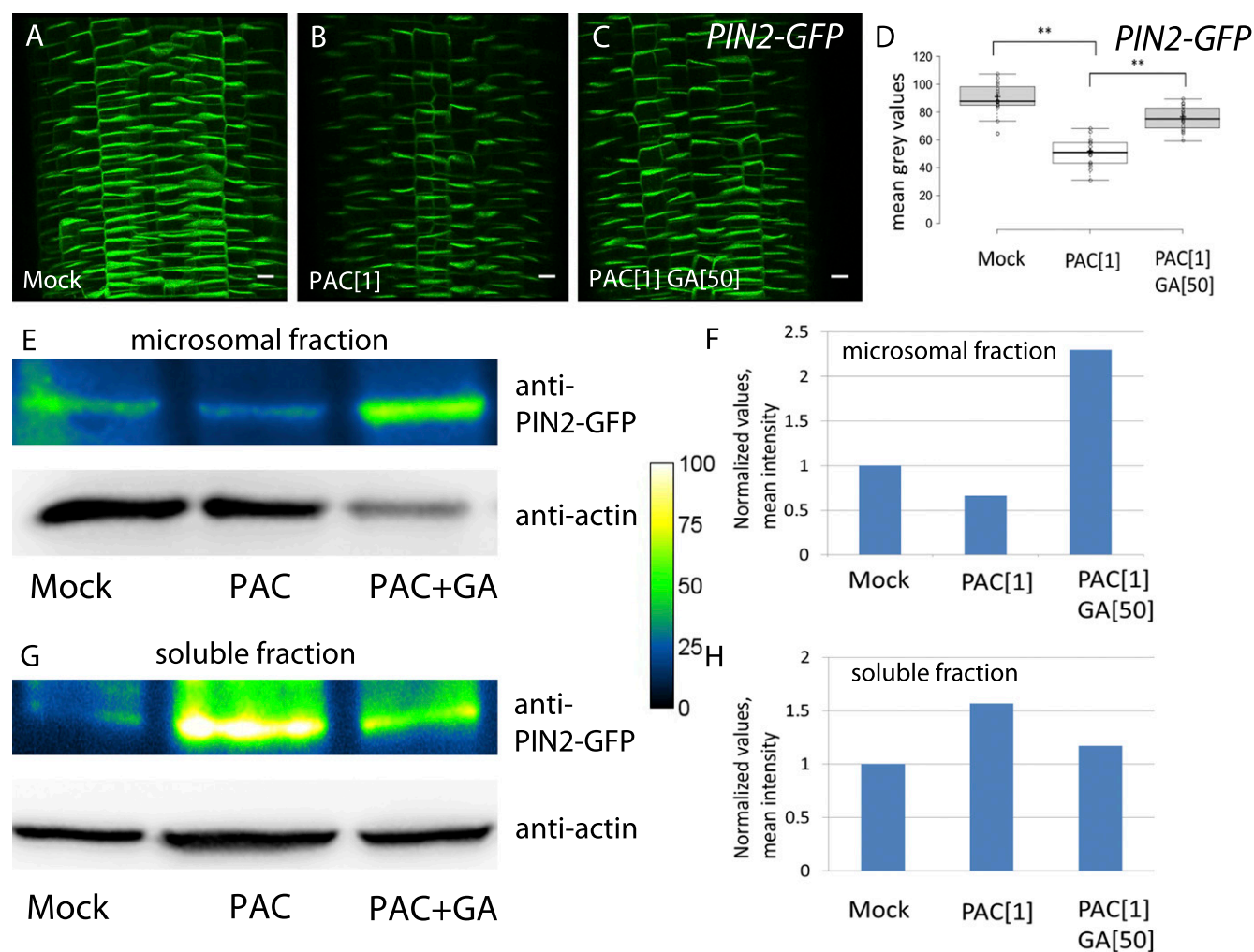


Fig. S1. GA availability led to PIN2-GFP abundance changes detected by confocal microscopy and Western blot. (A–C) PIN2-GFP signal at the PM in untreated seedlings (A), pretreated with 1 μ M PAC (B) and treated with 50 μ M GA for 4 h after PAC pretreatment (C). (D) Quantification of PIN2-GFP signals in the root epidermis (A–C). (E–H) Changes in PIN2-GFP protein levels detected by Western blot. Decrease in microsomal (membrane) PIN2-GFP protein upon PAC treatment and increase upon GA in *Arabidopsis* root tips (E). Enrichment of PIN2-GFP in soluble fraction coincided with PAC treatment and was reversed by GA (G). Western blot quantifications (F and H). Color code was used for PIN2-GFP amount visualization on Western blots. (Scale bar: 10 μ m.)

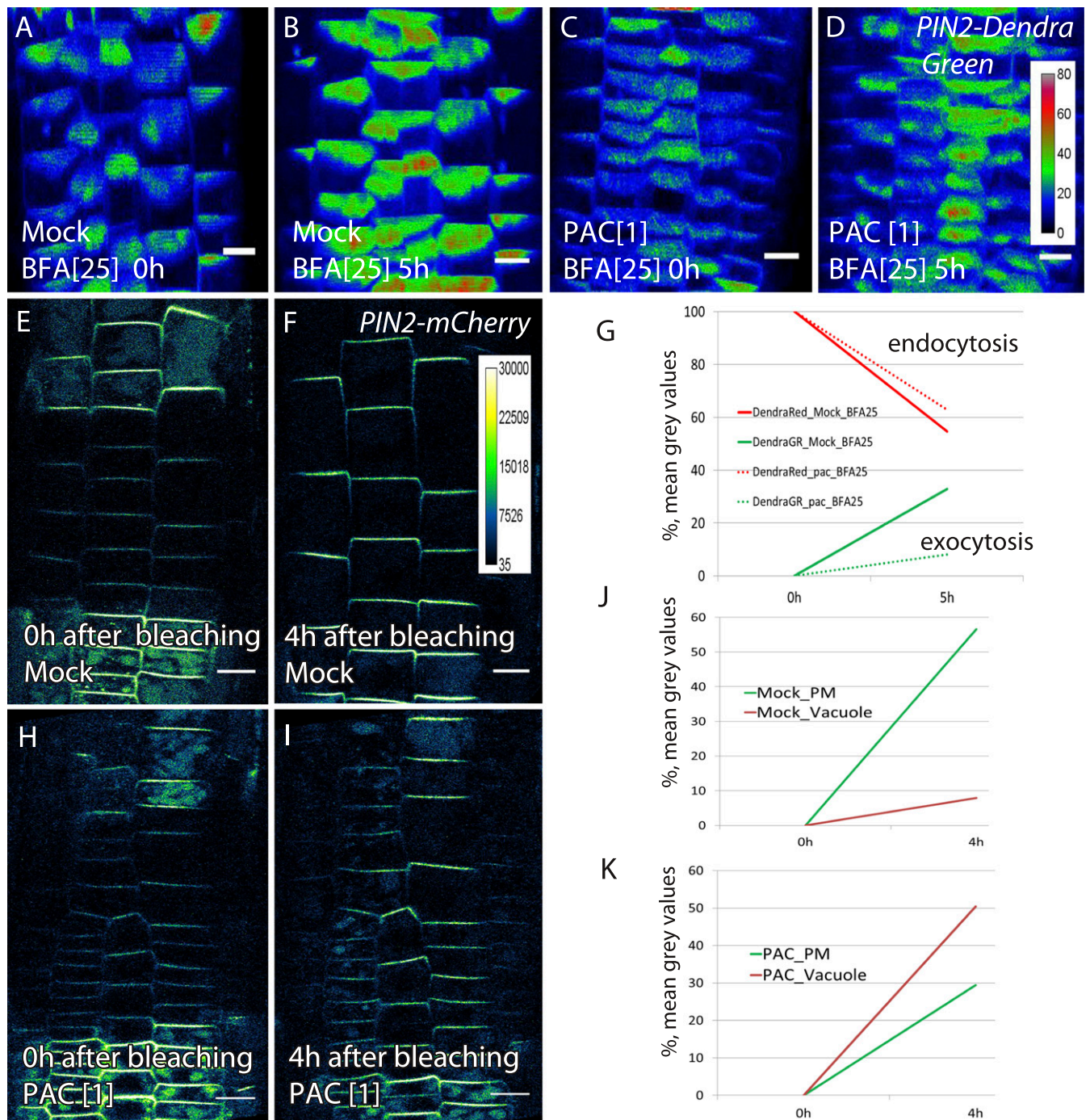


Fig. S2. GA effects on vacuolar delivery and recycling of the PM-located and de novo synthesized PIN2. (A–D) GA effects on the PIN2 vacuolar trafficking and exocytosis independent of BFA action. Photoconversion of PIN2-Dendra on seedlings grown on control medium (A and B) or 1 μ M PAC (C and D) plates and pretreated for 30 min with 25 μ M BFA. After 5 h of treatment with BFA, seedlings were imaged. Green signal recovery at the PM reflects de novo PIN2 delivery. Note the faster accumulation of de novo PIN2 at the PM in untreated (A and B) versus PAC-treated (C and D) seedlings. (G) Evaluation based on PIN2-Dendra red and green endocytosis and exocytosis rates in BFA-treated seedlings. (E, F, H, and I) PM localization of PIN2-mCherry 4 h after bleaching in untreated roots (E and F) compared with the vacuolar accumulation of PIN2-mCherry in PAC-treated roots (H and I). (J and K) Graphical representation of PM and vacuolar PIN2-mCherry distribution in mock (J) and PAC-treated (K) roots. Color code was used for PIN2-Dendra green and PIN2-mCherry intensity visualization. (Scale bar: 10 μ m.)

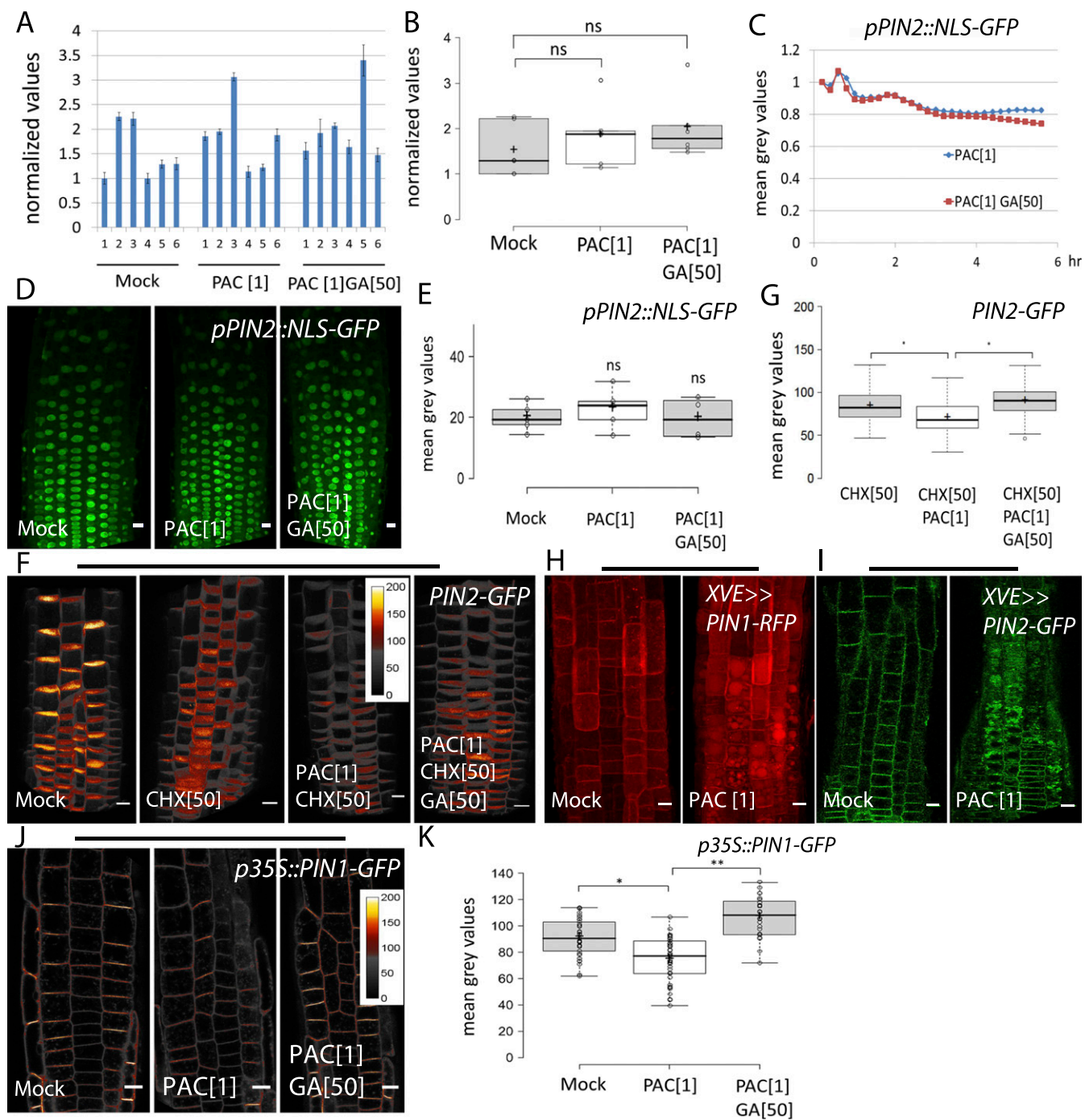


Fig. S3. GA effects on PIN-protein abundance. (A and B) qRT-PCR showed no changes in the levels of *PIN2* transcription upon PAC or GA treatments. Six independent mRNA repeats were included for each condition (A) and pooled together for more concise statistics (B). (C–E) GA did not affect the activity of the *PIN2* promoter. (C) Dynamics of *PIN2* promoter activity evaluated based on nuclear signal of *pPIN2::NLS-GFP* showing no differences in roots pretreated with PAC only versus PAC+GA-treated roots. (D and E) Unaffected *pPIN2::NLS-GFP* signal by PAC (1 d) or PAC+GA (1 d PAC+4 h GA) treatments. (F and G) Recovery of PAC-compromised *PIN2* level at the PM by GA in the presence of CHX, confirming a protein synthesis-independent regulation of PIN abundance by GA. (H–K) GA deficiency responsiveness of *PIN2* and *PIN1* proteins driven by estradiol-induced (XVE>>) and 35S-promoters. This confirms a PIN-promoter-independent regulation by GA and the effect on PIN protein abundance. (H and I) Vacuolar retargeting of XVE >> *PIN1-RFP* and XVE >> *PIN2-GFP* in PAC conditions. (J and K) Decrease in membrane stability of 35S::PIN1-GFP protein upon PAC and the reverse effect by GA (J). Signal quantification (K). Color code was used for *PIN2-GFP* (F) and 35S::PIN1-GFP (J) intensity visualization. (Scale bar: 10 μ m.)

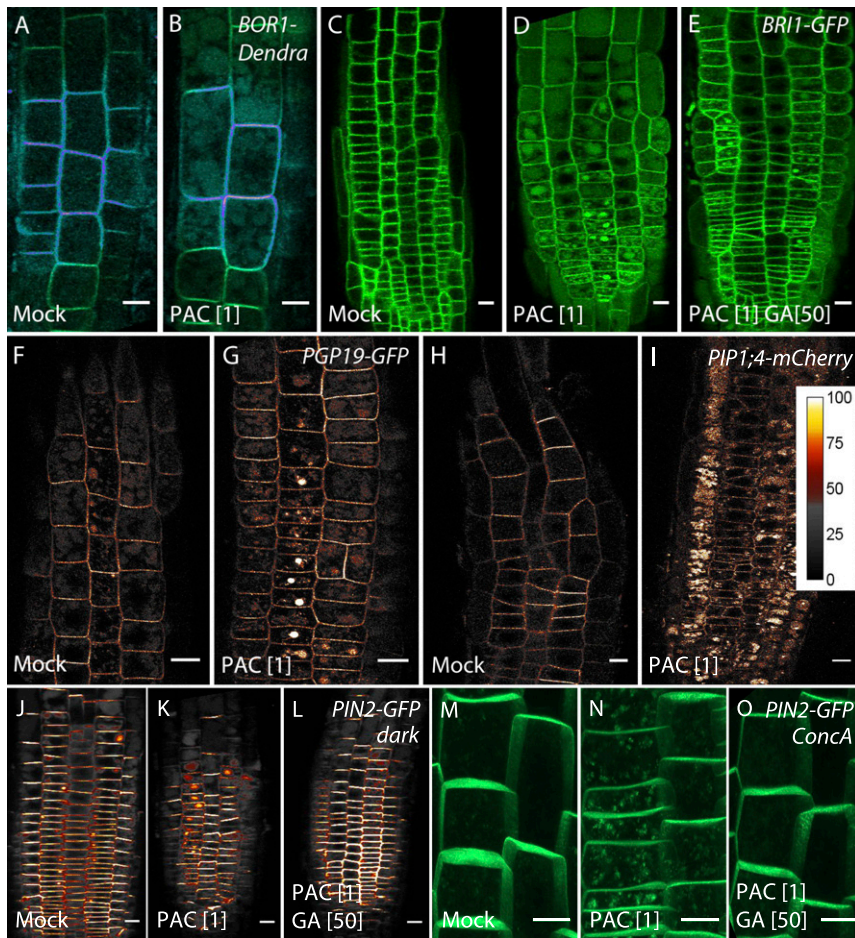


Fig. 54. GA effects on vacuolar targeting of different cargo proteins. (A and B) Increased vacuolar targeting of BOR1-Dendra in 1 μ M PAC-treated seedlings (B) compared with untreated mock (A). (C–E) Vacuolar localization of BRI1-GFP in 1 μ M PAC-treated seedlings (D) compared with prevalent PM-residing BRI1-GFP in mock (C) and 50 μ M GA-treated seedlings (E). (F–I) Increased vacuolar targeting of PGP19-GFP (G) and PIP1;4-mCherry (I) in PAC-treated seedlings compared with PM-accumulated PGP19-GFP (F) and PIP1;4-mCherry (H) in mock seedlings. (J–O) Visualization of increased vacuolar targeting of PIN2-GFP upon PAC treatment in dark (K) and 1 μ M conconamycin A (N) conditions in comparison with mock (J and M) and GA-treatment (L and O). Color code was used for PGP19-GFP, PIP1;4-mCherry, and PIN2-GFP (in dark) intensity visualization. (Scale bar: 10 μ m.)

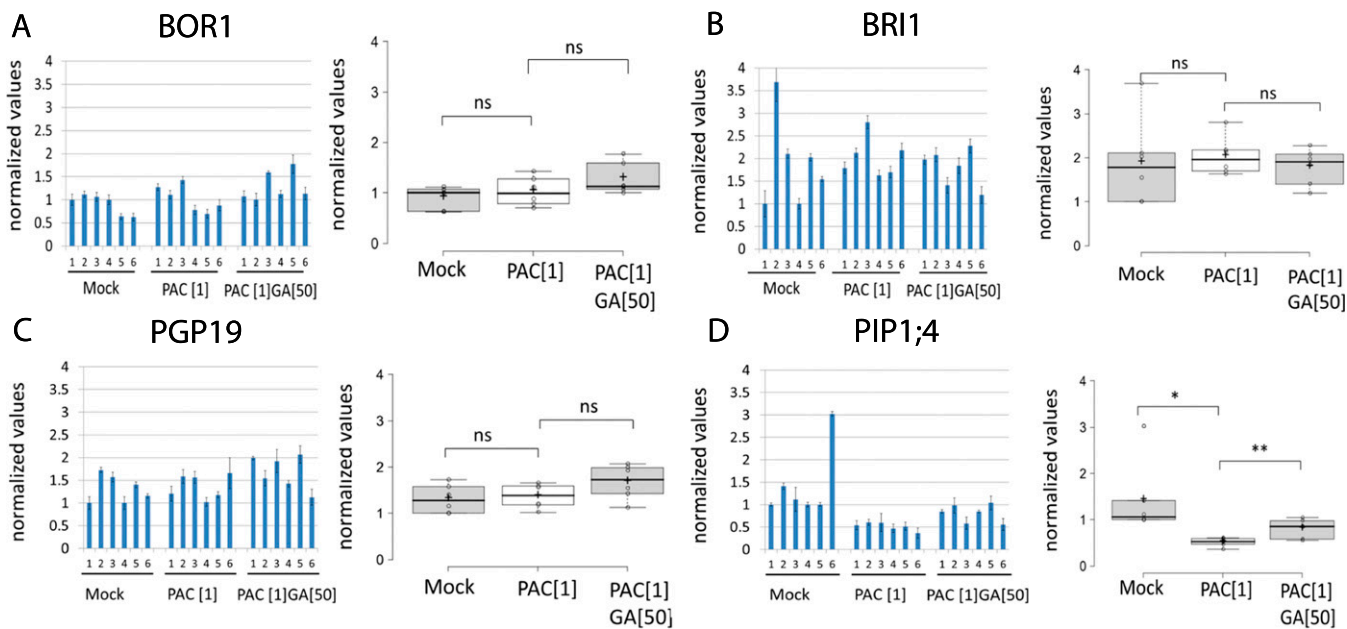


Fig. S5. qRT-PCR results of selected cargoes mostly unaffected by PAC or GA treatments. (A–C) Insignificantly different levels of mRNA of *BOR1* (A), *BRI1* (B), and *PGP19* (C) in mock, PAC, or GA-optimized conditions. (D) GA-dependent mRNA levels of *PIP1;4*. Six independent mRNA repeats were performed for each condition and pooled together for statistics. (E) Primers used for qRT-PCR of *PIN2* and other protein cargoes.

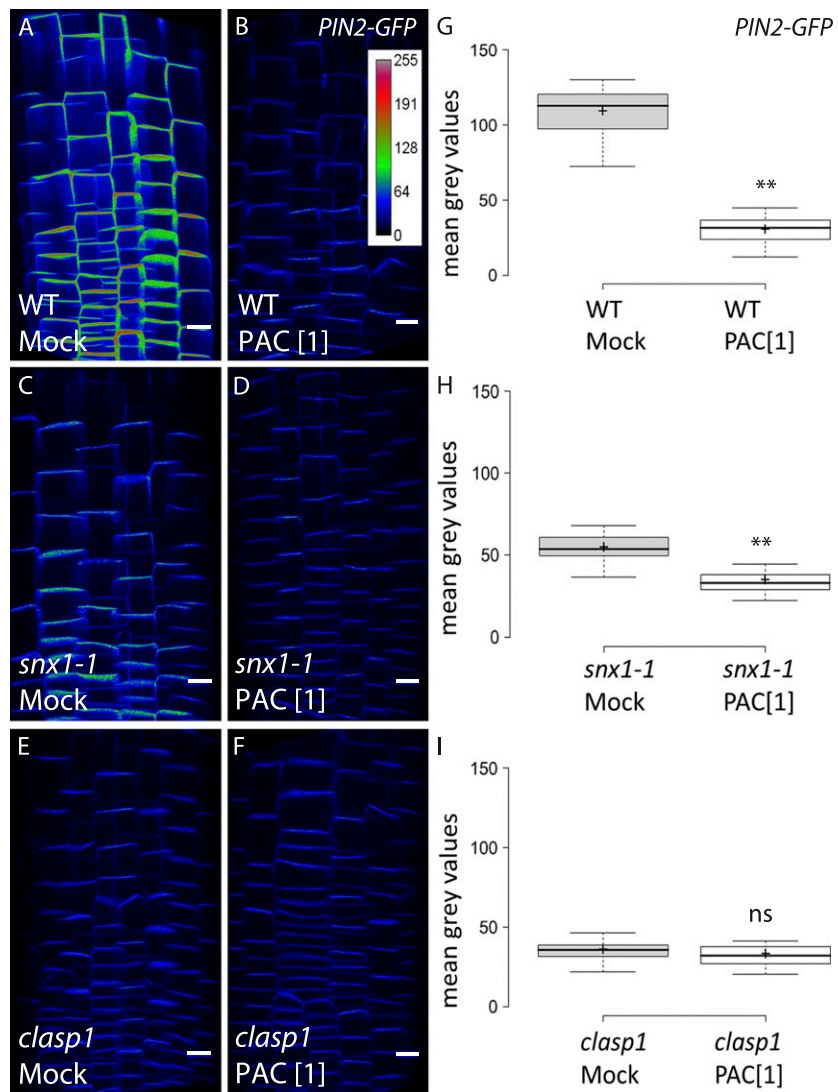


Fig. S6. Mutants compromised in SNX1 and CLASP1 proteins are less sensitive to PAC application. Decrease in PIN2-GFP PM levels was statistically significant but much less profound in *snx1-1* mutant plants treated with PAC (C, D, and H) compared with WT plants (A, B, and G). No significant changes in PIN2-GFP in *clasp1* mutant lines (E, F, and I). Color code was used for PIN2-GFP intensity visualization. (Scale bar: 10 μ m.)

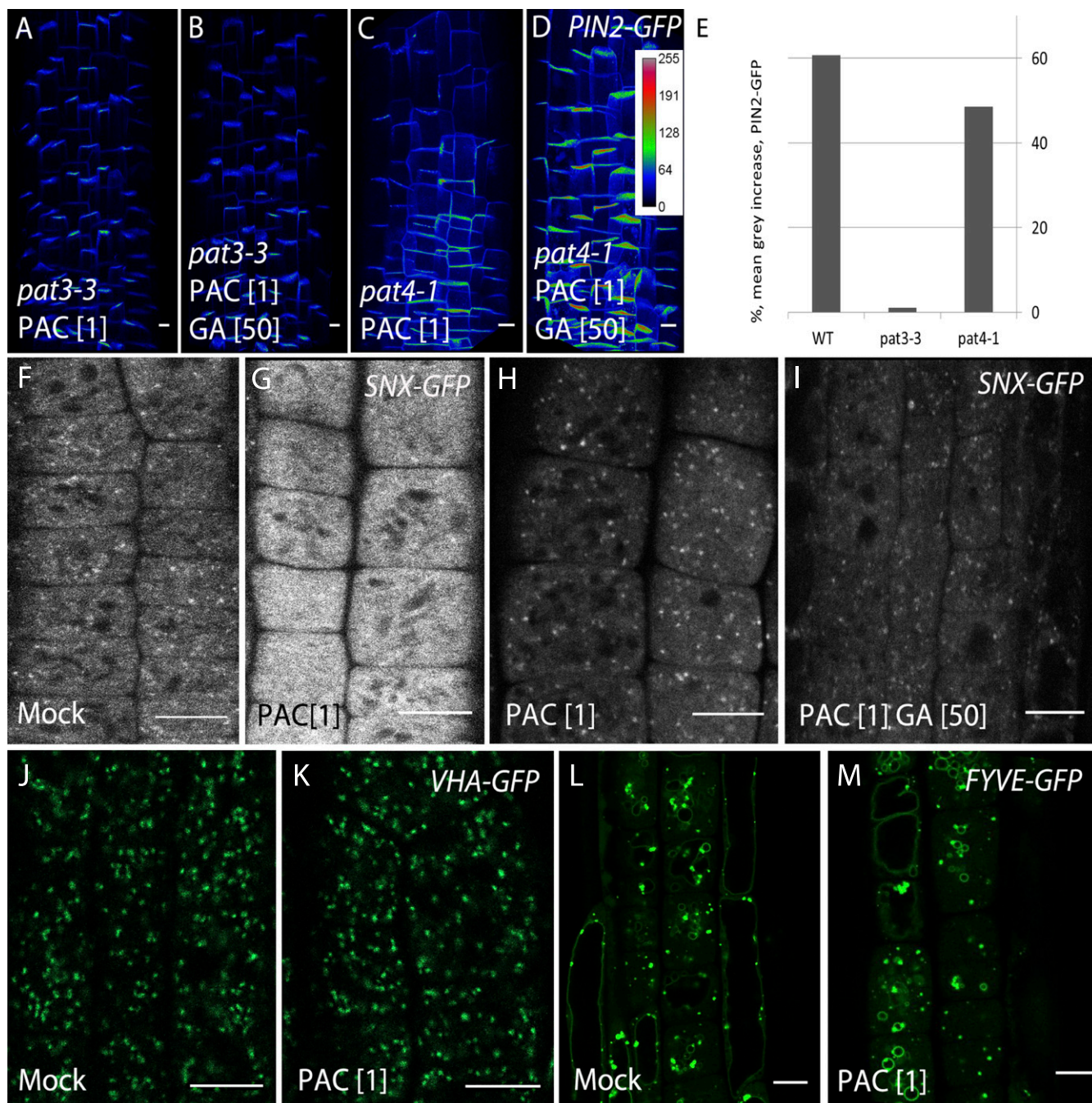


Fig. S7. GA targeting of a trafficking step upstream of the retromer-involving protein degradation. (A–E) Unrestored PIN2 at the PM after application of 50 μ M GA to the *pat3-3* roots pretreated with 1 μ M PAC (A and B) compared with efficiently restored amount of PIN2 at the PM in *pat4-1* after a similar treatment (C and D). Quantifications (E). (F and G) Increased cytosolic amount of SNX1-GFP in seedlings treated with 1 μ M PAC (G) compared with nontreated mock (F). (H and I) Decreased amount of abnormal endosomes within several hours of GA treatment (I) compared with PAC-treated seedlings (H). (J–M) GA deficiency lacking effects on the endosomal compartments labeled with VHA-GFP and FYVE-GFP, in comparison with SNX1-GFP. Unaffected endosomal localization of VHA-GFP (K) and FYVE-GFP (M) after 1 μ M PAC treatment compared with nontreated seedlings (J and L). Color code was used for PIN2-GFP signal visualization. (Scale bar: 10 μ m.)

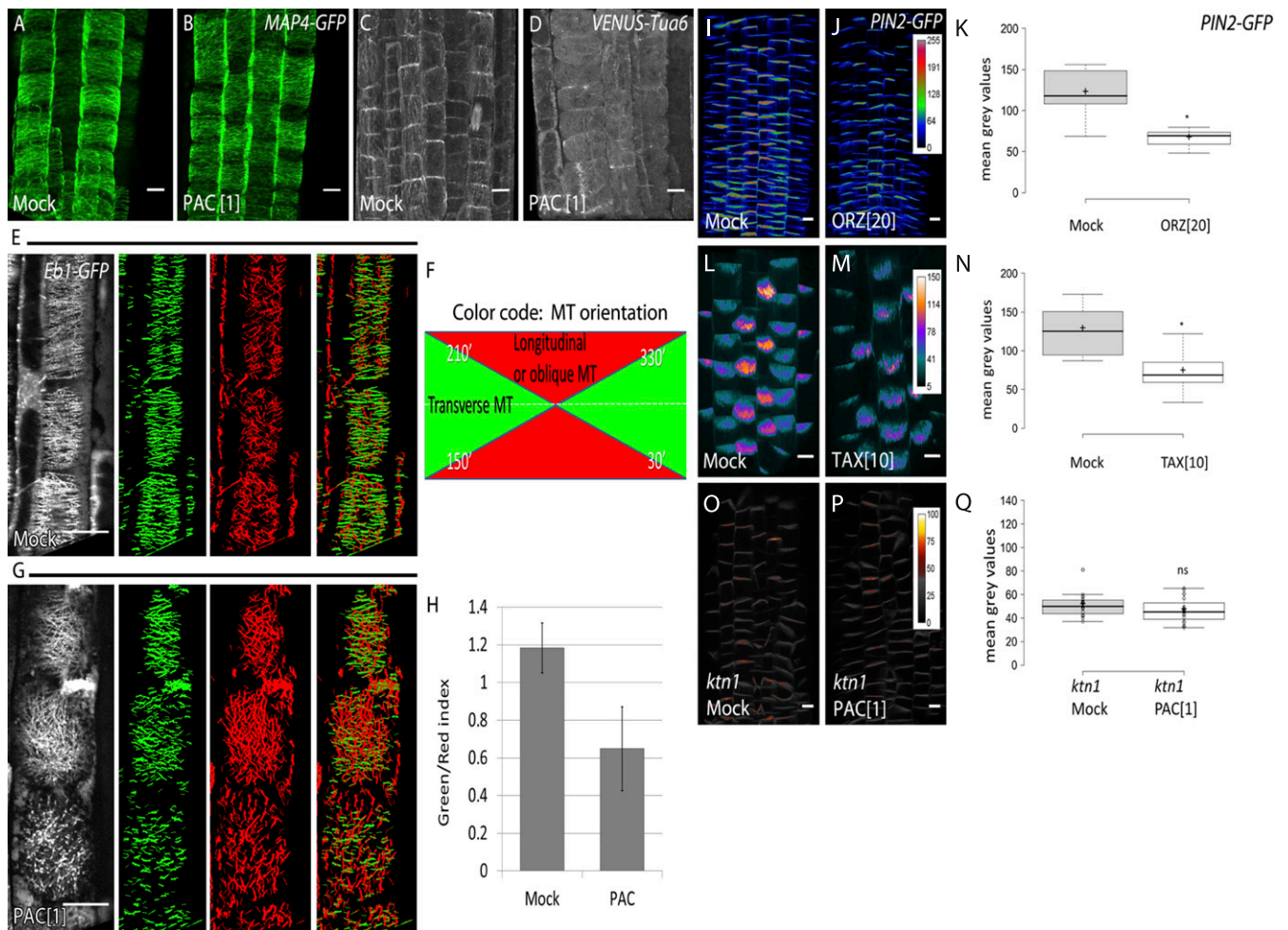


Fig. S8. MT are essential for GA action on PIN2 trafficking. (A and B) GA effect on MT. More randomized network of MTs in MAP4-GFP seedlings after treatment with 1 μ M PAC (B) compared with nontreated seedlings (A). (C and D) Confocal images of VENUS-TUA6 after prolonged PAC treatment of roots show an overall decrease in the MT network and increase in the fluorescent signal in the cytoplasm. (E–H) Reoriented microtubules labeled with Eb1b-GFP show enrichment in longitudinal or oblique direction (red color) upon PAC treatment (G) compared with more transversely oriented MTs in GA conditions (E). MT orientation was determined based on the angle of MTs toward the horizontal axis and color-coded accordingly (F). Green/red index indicates the ratio of transversally oriented MTs to oblique or longitudinal orientation in mock and PAC conditions (H). (I–Q) Depolymerization and stabilization of MTs affect PIN2 abundance. (I and J) Decrease in PIN2-GFP signal at PM after depolymerization of MTs with 20 μ M oryzalin. (L and M) Taxol-mediated stabilization of MTs leads to a significant drop of PIN2-GFP at PM. (O and P) No significant changes of PIN2-GFP in the *ktn1* mutant line upon PAC. (K, N, and Q) Quantifications of PIN2-GFP signal after oryzalin (K) and taxol (N) treatments and in *ktn1* mutant after PAC treatment (Q). Color code was used for PIN2-GFP signal visualization. (Scale bar: 10 μ m.)

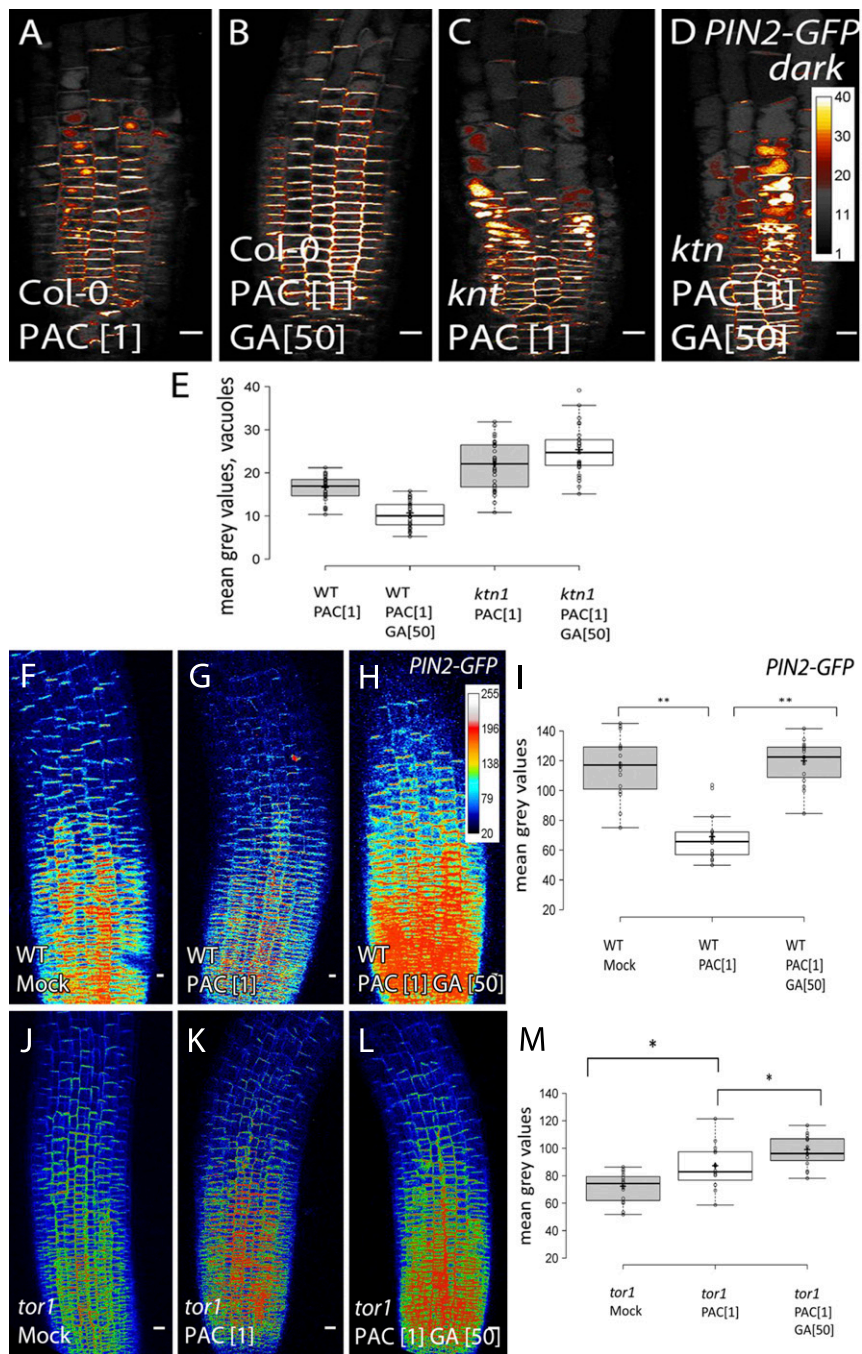


Fig. S9. *ktn1* and *tor1* mutants are insensitive to GA status. (A–D) Inability of *ktn1* mutant roots pretreated with PAC to decrease vacuolar PIN2 degradation after GA application (C and D) compared with GA in Col-0 plants (A and B). (E) Quantifications. (F–M) The decrease in PIN2-GFP signal, which was consistently observed in WT roots and rescued by GA application (F–I), was not observed in *tor1* mutant (J–M). On the contrary, a slight increase in PIN2-GFP level was observed on PAC-containing media in *tor1* roots (K). Color code was used for PIN2-GFP signal visualization. (Scale bar: 10 μ m.)

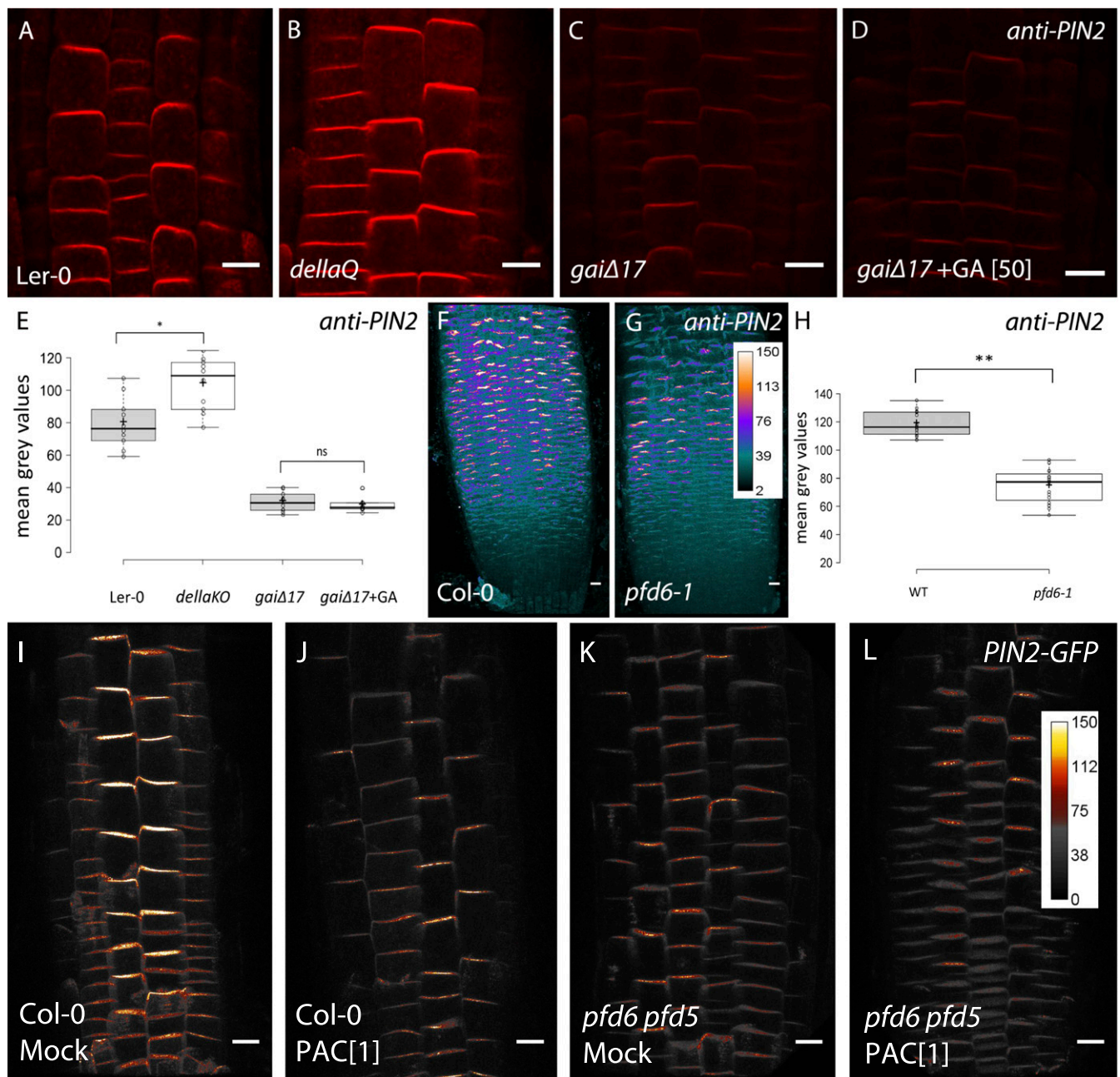


Fig. S10. DELLA and Prefoldin proteins are necessary for PIN2 level regulation. (A–D) Immunolocalization of PIN2 at the PM shows an increase of protein in *della* knockout seedlings (B) and a decrease in dominant-negative *gaiΔ17* mutants (C) compared with *Landsberg erecta-0* wild-type seedlings (A). (D) Insensitivity of *gaiΔ17* mutants to GA. (E) Quantifications. (F–H) Reduced PIN2 protein level in the *pfd6-1* mutant seedlings (G) compared with wild-type (F) seedlings by Z-stack maximum projection analysis of PIN2 immunolocalized samples. (H) Quantifications. (I–L) Mutants compromised in Prefoldin proteins are less sensitive to PAC application. No significant decrease in PIN2-GFP PM levels was detected in double *pfd5 pfd6* mutant plants treated with PAC (K and L) compared with WT plants (I and J). Color code was used for anti-PIN2 CY3 and PIN2-GFP signal visualization. (Scale bar: 10 μ m.)